

# PDT: Point Distribution Transformation with Diffusion Models

JIONGHAO WANG\*, Texas A&M University, USA

CHENG LIN\*<sup>†</sup>, The University of Hong Kong, China

YUAN LIU, The Hong Kong University of Science and Technology, China

RUI XU, The University of Hong Kong, China

ZHIYANG DOU, The University of Hong Kong, China

XIAO-XIAO LONG, Nanjing University, China

HAO-XIANG GUO, Skywork AI, Kunlun Inc., China

TAKU KOMURA, The University of Hong Kong, China

WENPING WANG and XIN LI<sup>†</sup>, Texas A&M University, USA

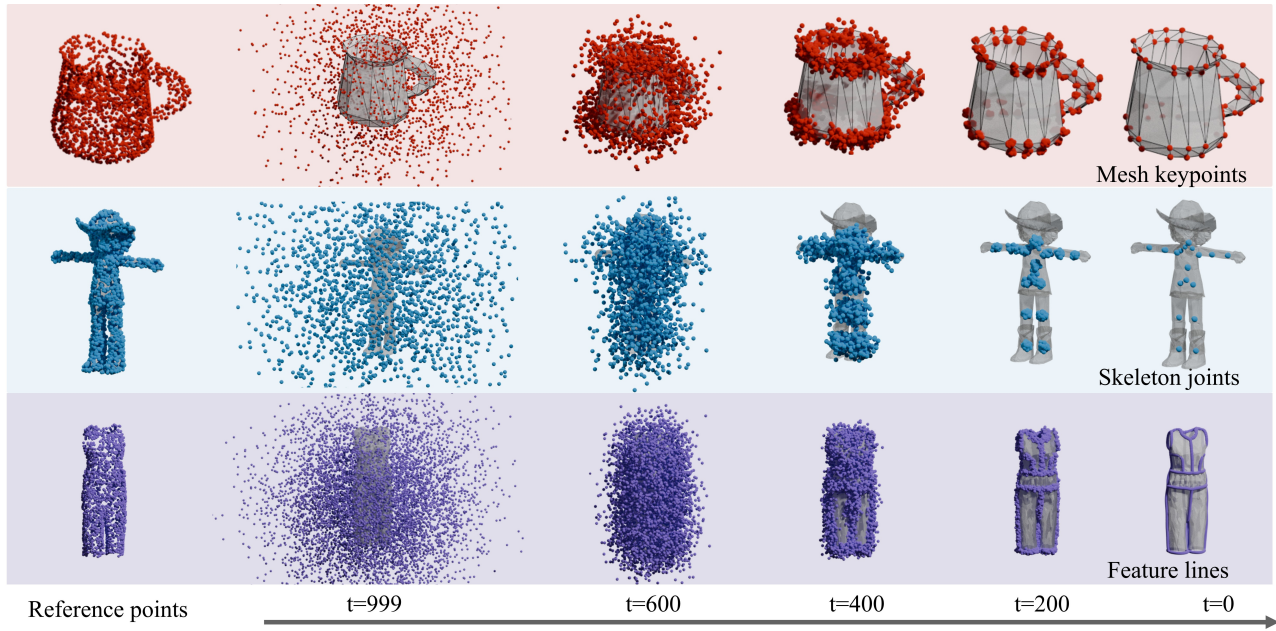


Fig. 1. Overview of PDT. PDT leverages a diffusion transformer-based architecture to transform Gaussian noise into semantically meaningful point distributions, guided by input reference points. We demonstrate the effectiveness of our approach across three structural representations: surface keypoints for artist-inspired meshes, inner skeletal joints for character rigging, and continuous feature lines for garment analysis. Note that meshes in this figure are only for reference.

\*Both authors contributed equally to this research.

<sup>†</sup>Corresponding authors.

Authors' Contact Information: Jionghao Wang, jionghao@tamu.edu, Texas A&M University, USA; Cheng Lin, chlin@connect.hku.hk, The University of Hong Kong, China; Yuan Liu, The Hong Kong University of Science and Technology, China, liuyuanwhuer@gmail.com; Rui Xu, ruixu1999@connect.hku.hk, The University of Hong Kong, China; Zhiyang Dou, zhiyang0@connect.hku.hk, The University of Hong Kong, China; Xiao-xiao Long, Nanjing University, China, xxlong@connect.hku.hk; Hao-xiang Guo, Skywork AI, Kunlun Inc., China, guohaoxiangxiang@gmail.com; Taku Komura, The University of Hong Kong, China, taku@cs.hku.hk; Wenping Wang, wenping@tamu.edu; Xin Li, xinli@tamu.edu, Texas A&M University, USA.

Permission to make digital or hard copies of all or part of this work for personal or classroom use is granted without fee provided that copies are not made or distributed for profit or commercial advantage and that copies bear this notice and the full citation on the first page. Copyrights for components of this work owned by others than the author(s) must be honored. Abstracting with credit is permitted. To copy otherwise, or republish, to post on servers or to redistribute to lists, requires prior specific permission and/or a fee. Request permissions from permissions@acm.org.

Point-based representations have consistently played a vital role in geometric data structures. Most point cloud learning and processing methods typically leverage the unordered and unconstrained nature to represent the underlying geometry of 3D shapes. However, how to extract meaningful structural information from unstructured point cloud distributions and transform them into semantically meaningful point distributions remains an under-explored problem. We present PDT, a novel framework for point distribution transformation with diffusion models. Given a set of input points, PDT learns to transform the point set from its original geometric distribution into a target distribution that is semantically meaningful. Our method utilizes diffusion models with novel architecture and learning strategy, which effectively correlates the source and the target distribution through a denoising process. Through extensive experiments, we show that our method successfully transforms input point clouds into various forms of structured

© 2025 Copyright held by the owner/author(s). Publication rights licensed to ACM.

ACM XXXX-XXXX/2025/7-ART

<https://doi.org/10.1145/nnnnnnn.nnnnnnn>

outputs - ranging from surface-aligned keypoints, and inner sparse joints to continuous feature lines. The results showcase our framework's ability to capture both geometric and semantic features, offering a powerful tool for various 3D geometry processing tasks where structured point distributions are desired. Code will be available at this link: [link](#).

CCS Concepts: • **Computing methodologies** → **Computer graphics**; **Computer vision**.

Additional Key Words and Phrases: Point Cloud, Diffusion, Remeshing, Rigging

#### ACM Reference Format:

Jionghao Wang, Cheng Lin, Yuan Liu, Rui Xu, Zhiyang Dou, Xiao-xiao Long, Hao-xiang Guo, Taku Komura, Wenping Wang, and Xin Li. 2025. PDT: Point Distribution Transformation with Diffusion Models. 1, 1 (July 2025), 11 pages. <https://doi.org/10.1145/nnnnnnn.nnnnnnn>

## 1 Introduction

Point-based 3D shape representations play a crucial role in characterizing geometry distributions. The flexibility, simplicity, and scalability of points make point clouds a fundamental component of geometric data structures. However, due to the unstructured and irregular nature of point clouds, effectively perceiving high-level semantic information from irregular point distributions and generating structurally meaningful representations remains a challenging task.

Existing methods often attempt to encode dense point clouds into implicit global features, followed by direct regression or classification to structured outputs (e.g., primitives, meshes, or skeletons). These approaches typically rely on deterministic feedforward mappings, which may struggle to capture the multimodal nature of semantic structures or maintain local geometric fidelity. In contrast, we propose a generative formulation that treats both the input and target structures as point distributions and learns to transform one into the other via guided denoising. This distribution-to-distribution mapping enables explicit pointwise correspondence, better handling structural ambiguity and producing compact, semantically meaningful outputs. As recent advances [Fu et al. 2024; He et al. 2024a] demonstrate, generative models offer greater flexibility and robustness for geometry reasoning tasks. While diffusion models have shown strong performance in 3D generation, their potential for transforming point distributions into structured representations remains underexplored—this work aims to fill that gap.

In this paper, we introduce a novel framework, named PDT, for point distribution transformation using diffusion models. Given a set of input points representing the shape geometry, our method learns to transform the points from their original surface distribution, where the input point cloud is viewed as samples drawn from the underlying surface probability distribution, into a semantically meaningful target distribution. The target structured points, such as keypoints or feature lines, are treated as a separate probability distribution in 3D space. We establish a probabilistic mapping between the two distributions by injecting Gaussian noise to the input points and learning to progressively denoise them toward the target points, correlating the surface geometry distribution and the target structure distribution through explicit per-point guidance.

Our method is simple yet effective overall, with several key designs that make it well-suited for transformation between different

point distributions. First, by introducing explicit correspondences between each noisy input point and a target structure point, we enable the denoising process to effectively perceive local geometry in specific regions, thereby generating target points that align with the local structures. Second, since the distribution of semantically structured points is typically compact and sparse, while the input point distribution is usually dense, our method should accurately map each point from an excessive point set to a precise location within a sparse set of target points. To enhance the denoising process's ability to capture fine-grained details, we carefully design a noise schedule that strengthens the learning of local details. Additionally, we introduce a gradient-guided strategy during inference, which makes the point distribution transformation more controllable and precise.

We demonstrate our method in three tasks where the input points are transformed into different semantically meaningful target distributions reflecting distinct structural priors: 1) surface-aligned mesh keypoints; 2) inner skeletal joints; and 3) continuous feature lines. These three distributions reflect different structural dependencies between the target and the source point geometry. Through extensive experiments, we validate the strong structural prediction and perception capabilities of our method across these tasks, demonstrating its ability to effectively generate semantically meaningful point distributions. This, in turn, facilitates improvements in corresponding downstream tasks. Our results highlight that the proposed method serves as a general-purpose framework for point distribution transformation, exhibiting remarkable diversity, versatility, and potential for further extension.

## 2 Related Work

### 2.1 Learning Point-based Transformations

Point-based transformation methods have been an active area of research in 3D geometry processing. Early approaches focused on specific geometric transformations, such as surface-to-skeleton mapping [Lin et al. 2021; Yin et al. 2018] and point cloud completion [Wen et al. 2021]. While these methods demonstrate effectiveness in their targeted domains, their reliance on deterministic feed-forward networks limits their capability to model complex distribution patterns and capture intricate geometric relationships. While methods such as VoteNet [Qi et al. 2019] and Robust Symmetry Detection via Riemannian Langevin Dynamics [Je et al. 2024] excel at extracting sparse structures for specific tasks like object and symmetry detection, our approach offers a more flexible pipeline. Through task-specific training, it can effectively address objectives ranging from highly sparse to relatively dense, unlike methods inherently tailored to sparse outputs.

Recent advances in denoising diffusion probabilistic models (DDPM) [Ho et al. 2020] and their variants [Nichol and Dhariwal 2021; Peebles and Xie 2023] have shown remarkable success in various 3D generation tasks. These approaches have been effectively applied to diverse 3D representations, including 3D Gaussians [Tang et al. 2025], neural fields [Yu et al. 2023; Zhang et al. 2023, 2024], and multi-view images [Li et al. 2024; Long et al. 2024]. In the context of point clouds specifically, several works have leveraged diffusion models for generation tasks, such as PVD [Zhou et al. 2021], Point-E [Nichol

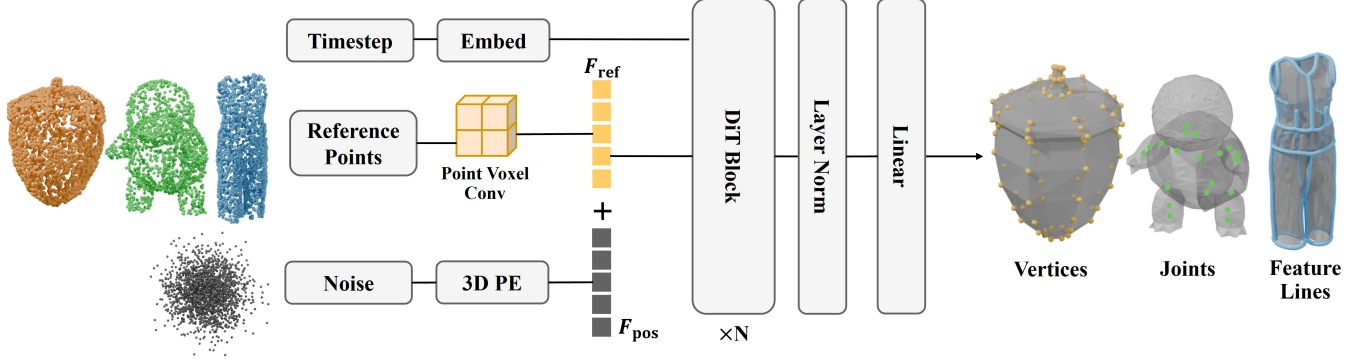


Fig. 2. Architecture overview of our PDT. The model extracts per-point features  $F_{\text{ref}}$  with Point Voxel Conv(PVCNN) [Liu et al. 2019] from input reference points and associates them with corresponding noisy points through adding its positional encoding features  $F_{\text{pos}}$  through a learnable positional embedding(3D PE). The combined features and timestep embeddings are processed through a series of DiT layers to learn the distribution transformation.

et al. 2022], and LION [Vahdat et al. 2022]. Notably, DiT-3D [Mo et al. 2023] pioneered the integration of the DiT architecture [Peebles and Xie 2023] into point cloud processing.

Of particular relevance to our work is Geometry Distribution [Biao et al. 2024], which demonstrates the capability of diffusion models to learn and represent surface point distributions. While they focus on modeling individual distributions as shape representations, our work extends this concept by learning the transformations between different point distributions.

## 2.2 Structured Representations

We examine three fundamental types of structured point-based representations: surface keypoints, skeletal joints, and garment feature lines, each serving distinct purposes in 3D geometry processing and computer graphics applications.

**2.2.1 Surface keypoints and remeshing.** Surface keypoints serve as critical geometric landmarks that capture the essential structural and semantic features of 3D shapes. The generation of semantically meaningful surface keypoints represents a fundamental challenge in geometric processing, particularly for creating artist-inspired meshes. Traditional remeshing approaches, including Quadric Error Metrics (QEM) [Chen et al. 2023; Garland and Heckbert 1997; Liu et al. 2023; Ozaki et al. 2015; Panchal and Jayaswal 2022; Wei and Lou 2010] and Centroidal Voronoi Tessellation (CVT) [Du et al. 1999, 2018; Edwards et al. 2013; Lévy and Liu 2010; Sun et al. 2011; Wang et al. 2018; Yan and Wonka 2015], primarily focus on geometric feature preservation through optimization-based techniques. While these methods excel at generating isotropic meshes, they often fail to capture the semantic understanding inherent in artist-created representations.

Recently, a series of methods for compact mesh generation have demonstrated impressive results [Achiam et al. 2023; Chen et al. 2024a,b; Wang et al. 2024; Weng et al. 2024]. These methods predominantly operate by treating mesh faces as token sequences and generating them through autoregressive processes. Their share a similar idea of treating mesh faces as token sequences and generating them autoregressively. In contrast, we ventured down a

completely new and distinct path by directly generating the 3D guiding keypoints that serve as a foundation followed by a simple remeshing process.

**2.2.2 Skeletal joints.** Automatic rigging is an important task and can reduce the manual effort required from artists in character creation and animation processes. Skeletal joints serve as fundamental control points for character rigging, enabling subsequent animation capabilities [Liao et al. 2022]. Traditional approaches, such as Pinocchio [Baran and Popović 2007], rely on fixed templates, limiting their ability to accommodate diverse skeletal structures. While learning-based methods such as RigNet [Xu et al. 2020] have demonstrated promising results in joint prediction, their reliance on deterministic feed-forward networks constrains their ability to model complex skeletal distribution patterns and capture intricate anatomical relationships. In contrast, our PDT framework leveraging diffusion models demonstrates superior precision and robustness.

**2.2.3 Garment feature lines.** Feature lines in garment design serve as critical elements for understanding garment construction, defining style characteristics, and analyzing pattern layouts. While recent research has made significant progress in garment generation with patterns [He et al. 2024b; Korosteleva and Sorkine-Hornung 2023; Liu et al. 2024; Long et al. 2023; Yu et al. 2023], the specific challenge of extracting and representing garment feature lines for pattern understanding remains largely unexplored.

Our framework uniquely addresses the challenges inherent in each of these structured representations by providing a unified approach to point distribution transformation, enabling the capture of both geometric and semantic relationships across different domains of 3D shape analysis.

## 3 Methodology

Given a reference point cloud  $\mathbf{P}_{\text{ref}} = \{p_{\text{ref}}^i \in \mathbb{R}^3 \mid i = 1, \dots, N\}$  sampled from a source surface distribution  $p_S(\mathbf{x})$ , our objective is to generate a corresponding set of target points  $\mathbf{P}_{\text{target}} = \{p_{\text{target}}^i \in \mathbb{R}^3 \mid i = 1, \dots, N\}$  that characterize structural features. For training, we establish correspondences between each reference point  $p_{\text{ref}}^i$

in  $\mathbf{P}_{\text{ref}}$  and its associated target point  $p_{\text{target}}^i$  in the ground truth structure, defined through a matching function  $\mathcal{F} : \mathbb{R}^3 \rightarrow \mathbb{R}^3$  that maps reference points to their nearest target points. Our diffusion model learns to transform points from an initial Gaussian noise distribution towards these target positions through a guided denoising process. Specifically, we maintain explicit associations between each point in the diffusion trajectory and its corresponding reference point, enabling the model to learn the underlying geometric relationships that govern the transformation from  $p_S(\mathbf{x})$  to  $p_T(\mathbf{x})$ .

### 3.1 DDPM revisited

We first revisit DDPMs and diffusion models. In Denoising Diffusion Probabilistic Models (DDPM) [Ho et al. 2020], the diffusion model is formulated as a pair of processes: a forward noising process and a reverse denoising process. The forward process gradually adds Gaussian noise to the original data  $\mathbf{x}_0$  through a sequence of steps, defined by the transition probability  $q(\mathbf{x}_t | \mathbf{x}_{t-1}) = \mathcal{N}(\mathbf{x}_t; \sqrt{1 - \beta_t} \mathbf{x}_{t-1}, \beta_t \mathbf{I})$ , where  $\beta_t$  represents the scheduled noise variance at each timestep, with values between 0 and 1. In the reverse process, the diffusion model is trained to learn a denoising network parameterized by  $\theta$ , which inverts the forward process to recover the original data. This reverse process is defined as  $p_\theta(\mathbf{x}_{t-1} | \mathbf{x}_t) = \mathcal{N}(\mathbf{x}_{t-1}; \mu_\theta(\mathbf{x}_t, t), \sigma_t^2 \mathbf{I})$ , where the network  $\mu_\theta$  predicts the mean of the denoised distribution. In this formulation,  $x_t$  can be sampled at time step  $t$  in the form of:  $q(\mathbf{x}_t | \mathbf{x}_0) := \mathcal{N}(\mathbf{x}_t; \sqrt{\bar{\alpha}_t} \mathbf{x}_0, (1 - \bar{\alpha}_t) \mathbf{I})$ , thus we have:

$$\mathbf{x}_t := \sqrt{\bar{\alpha}_t} \mathbf{x}_0 + \sqrt{1 - \bar{\alpha}_t} \epsilon, \quad \text{where } \epsilon \sim \mathcal{N}(\mathbf{0}, \mathbf{I}) \quad (1)$$

where  $\alpha_t := 1 - \beta_t$  and  $\bar{\alpha}_t := \prod_{s=1}^t \alpha_s$ .

### 3.2 Geometry distribution transformation

Our objective is to use diffusion models to learn the transformation from an arbitrary surface point distribution to a semantically meaningful target point distribution. In this paper, we demonstrate the transformation of surface sample points into three typical distributions: mesh key points, inner skeletal points, and feature line points. Inspired by Geometry Distributions [Biao et al. 2024], our method introduces a point-wise guided diffusion framework where each point in the diffusion process maintains an explicit correspondence with a sampled reference point from the source surface. Unlike previous methods where conditioning is performed with the reference point cloud as a whole, our explicit per-point correspondence provides a flexible geometric representation where any sampling density from the source surface yields valid transformations while preserving geometric fidelity.

We formalize our geometric transformation framework as a probabilistic mapping between two distributions: a source distribution  $p_S(\mathbf{x})$  that characterizes the underlying surface geometry, and a target geometry distribution  $p_T(\mathbf{x})$  that represents structural features. Given the surface distribution  $p_S(\mathbf{x})$ , we sample a set of reference points  $\mathbf{P}_{\text{ref}} \sim p_S(\mathbf{x})$ , and use this point set to guide a diffusion denoiser  $\epsilon_\theta(\mathbf{x}_t, t, \mathbf{P}_{\text{ref}})$ .

Following the denoising diffusion probabilistic model framework [Ho et al. 2020], we use the identical forward progress to corrupt the initial distribution. The reverse process learns a parametric model

$\epsilon_\theta(\mathbf{x}_t, t, \mathbf{P}_{\text{ref}})$  that predicts the noise components conditioned on both the current state  $\mathbf{x}_t$  and the reference points  $\mathbf{P}_{\text{ref}}$ . This enables guided denoising through the conditional probability  $p_\theta(\mathbf{x}_{t-1} | \mathbf{x}_t, \mathbf{P}_{\text{ref}})$ . During inference, the process begins with  $\mathbf{x}_T \sim \mathcal{N}(\mathbf{0}, \mathbf{I})$  and iteratively samples points that converge to the target distribution  $p_T(\mathbf{x})$ , while the conditioning on  $\mathbf{P}_{\text{ref}}$  ensures preservation of geometric relationships with the source surface throughout the generation trajectory.

### 3.3 Model design

As shown in Fig. 2, our model architecture is designed to effectively learn the geometry distribution transform between source and target point distributions while maintaining explicit point-wise correspondences throughout the diffusion process. Our design integrates a diffusion transformer (DiT) [Peebles and Xie 2023] framework with a Point Voxel CNN (PVCNN) [Liu et al. 2019] feature extractor, where the PVCNN enables robust point feature extraction and the Diffusion Transformer guides the denoising process. This design choice is motivated by two key requirements from our problem formulation: (1) the need to process and maintain point-wise relationships between reference points  $\mathbf{P}_{\text{ref}}$  and their corresponding target positions, and (2) the necessity to condition the denoising process on these geometric relationships. Accordingly, PVCNN efficiently extracts per-point features that capture local geometric context from the reference point cloud, while DiT's transformer architecture enables effective modeling of the conditional probability  $p_\theta(\mathbf{x}_{t-1} | \mathbf{x}_t, \mathbf{P}_{\text{ref}})$  through its self-attention mechanisms. This combination allows our model to learn the underlying geometric relationships that govern the transformation from  $p_S(\mathbf{x})$  to  $p_T(\mathbf{x})$  while preserving point-wise correspondences throughout the diffusion trajectory.

We start by extracting per-point features from the reference point cloud  $\mathbf{P}_{\text{ref}}$  using PVCNN, resulting in a feature matrix  $\mathbf{F}_{\text{ref}} \in \mathbb{R}^{N \times C}$ , where  $N$  represents the number of points and  $C$  is the dimensionality of the features. These extracted features act as references for guiding the noised key points toward their target structural positions.

A learnable positional embedding function  $\mathbf{E}_{\text{pos}} : \mathbb{R}^3 \rightarrow \mathbb{R}^C$  is applied. It takes the  $(x, y, z)$  coordinates of each point in  $\mathbf{P}_{\text{ref}}$  and outputs a corresponding feature embedding for each individual point. The extracted per-point features  $\mathbf{F}_{\text{ref}} \in \mathbb{R}^{N \times C}$ , together with the positional embeddings  $\mathbf{F}_{\text{pos}} = \mathbf{E}_{\text{pos}}(\mathbf{P}_{\text{ref}})$ , are combined to form the input tokens  $\mathbf{F}_{\text{in}} = \mathbf{F}_{\text{ref}} + \mathbf{F}_{\text{pos}}$  for the DiT.

Additionally, we incorporate a timestep embedding  $\mathbf{F}_{\text{time}} \in \mathbb{R}^C$  as a conditioning signal for the DiT, consistent with the original DiT structure. Each DiT block consists of two main branches: a self-attention pathway and a feed-forward network (FFN) pathway. The self-attention branch enables global information exchange across all points, while the FFN branch processes point features independently. Both branches are augmented with adaptive layer normalization and scale-shift operations conditioned on timestep embeddings.

### 3.4 Noise schedule

The noise schedule in a diffusion model, represented by the sequence  $\beta_t$ , determines the Gaussian noise level added at each timestep in the forward process. The schedule is designed to progressively corrupt



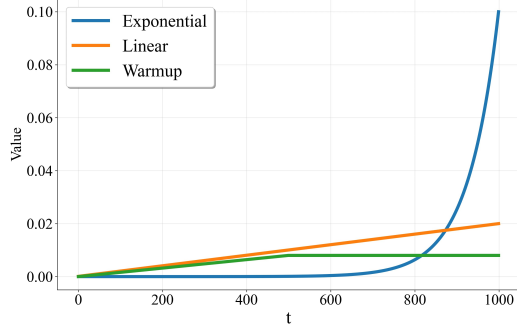


Fig. 3. Comparison of different noise schedules. Our exponential schedule (blue) exhibits notably smaller  $\beta_t$  values at lower timesteps, enabling more precise control during final denoising stages.

the original data distribution until it approximates a standard Gaussian distribution. In the original DDPM [Ho et al. 2020], a simple linear schedule for  $\beta_t$  was employed.

The semantically meaningful points (e.g., key points, joints) are typically compact with fewer vertices, while the number of sampling points is relatively high. Therefore, the ideal scenario for the sampling points is to be densely clustered around the few vertices of the structured mesh. This imposes high demands on the convergence accuracy of the diffusion model. In our experiments, however, we observe that conventional noise schedules result in “fuzzy” outputs, where points fail to converge precisely on the target vertices. We identify the cause as the relatively high noise levels near the end of the diffusion process (at timesteps close to  $t = 0$ ), where generated vertices should ideally form tight clusters. Large noise scales at these later stages introduce excessive variance, preventing the generated points from converging accurately.

To address this, we modified the noise schedule by setting the  $\beta_t$  values close to  $t = 0$  to be significantly smaller. This adjustment reduces variance at critical points in the denoising process, allowing the generated vertex positions to converge more precisely. As shown in the accompanying graph Fig. 3, our modified schedule has smaller  $\beta_t$  values at smaller  $t$  steps, spending more effort on fine-grained details of our denoising process.

Under this design, however, the value of  $\beta_t$  close to  $t = 1000$  must be significantly larger to ensure proper training. Recall the sampling equation 1. To minimize the discrepancy between training and inference distributions, we need the variance  $\sqrt{1 - \bar{\alpha}_t}$  to approach 1 at large  $t$ , ensuring the forward process properly approximates a standard Gaussian distribution. We determined the terminal value to be  $\beta_t = 0.1$ , yielding  $\sqrt{1 - \bar{\alpha}_t} \approx 0.9998$ , which empirically provides stable training while maintaining sufficient proximity to the standard Gaussian. Through experimentation, we find that our modified noise schedule robustly produces precise point clusters.

### 3.5 Sampling gradient adjustment

Once the distribution transformation model is trained, during inference, we can impose constraints on the direction of distribution convergence to guide the target point distribution toward our desired outcome and thus enhance geometric precision, we introduce a

sampling gradient adjustment (SGA) strategy that can be customized for different target distributions.

The sampling process, detailed in Algorithm 1, introduces a correction gradient term at each denoising step. Inspired by [Chung et al. 2022], for a given timestep  $t$ , we compute a geometry-aware gradient based on the current estimated positions  $\hat{\mathbf{x}}_0$  and target geometric constraints. This gradient is then applied with a step size  $\rho$  to guide points toward geometrically optimal positions.

---

#### Algorithm 1 Sampling gradient adjustment for surface keypoints

---

**Require:**  $T, \{\alpha_t\}_{t=1}^T, \{\sigma_t\}_{t=1}^T, \mathcal{M}, \mathbf{P}_{\text{ref}}, \rho$   
 $\mathbf{x}_T \leftarrow \mathcal{N}(0, I)$   
**for**  $t = T$  **down to** 1 **do**  
 $\mathbf{z} \leftarrow \mathcal{N}(0, I)$  if  $t > 1$ , else  $\mathbf{z} = 0$   
 $\hat{\mathbf{x}}_0 \leftarrow \frac{\mathbf{x}_t - \sqrt{1 - \bar{\alpha}_t} \epsilon_{\theta}(\mathbf{x}_t, t)}{\sqrt{\bar{\alpha}_t}}$   
Find the closest point  $\mathbf{c} \in \mathcal{M}$  to  $\hat{\mathbf{x}}_0$   
Calculate adjustment gradient:  $\nabla_{\mathbf{x}_t} = \|\hat{\mathbf{x}}_0 - \mathbf{c}\|_2^2$   
 $\mathbf{x}'_{t-1} \leftarrow \frac{1}{\sqrt{\alpha_t}} \left( \mathbf{x}_t - \frac{1 - \alpha_t}{\sqrt{1 - \bar{\alpha}_t}} \epsilon_{\theta}(\mathbf{x}_t, t, \mathbf{P}_{\text{ref}}) \right) + \sigma_t \mathbf{z}$   
 $\mathbf{x}_{t-1} \leftarrow \mathbf{x}'_{t-1} - \rho \nabla_{\mathbf{x}_t}$   
**end for**  
**return**  $\mathbf{x}_0$

---

We can impose different constraints based on the characteristics of the target distributions. For example, if the target distribution is surface-aligned (e.g., mesh keypoints), the gradient guides points toward the input surface  $\mathcal{M}$ , ensuring generated vertices maintain close surface alignment. The gradient is computed as the squared distance between each predicted point and its closest surface point. If the target point distribution is inside the surface (e.g., inner skeletal points), we can optionally use directional adjustment such as reverse normal direction to guide joints closer to the medial axis.

## 4 Applications

To demonstrate our method, we use three representative tasks where input points are transformed into distinct semantically meaningful geometric distributions: 1) surface-aligned mesh keypoints, 2) inner skeletal joints, and 3) continuous feature lines. These distributions highlight the varying structural relationships between the target and source point geometries.

### 4.1 Surface mesh keypoints

The emergence of advanced 3D generation techniques has led to increasingly detailed and complex meshes. However, these high-resolution outputs often lack the carefully crafted structural properties that characterize artist-created meshes, making them less suitable for practical applications in animation, gaming, and interactive media. Our first application addresses this challenge by transforming dense surface samples into strategic vertex positions that guide mesh simplification toward artist-like results. Rather than solving remeshing directly, our focus is on generating semantically meaningful vertex proposals that guide classical simplification algorithms, bridging learning-based prediction with traditional geometry processing.

Given an input mesh  $\mathcal{M}$ , we first sample a dense set of reference points  $\mathbf{P}_{\text{ref}}$  from its surface. Our PDT framework then transforms these points into a set of predicted vertex positions that capture key geometric features while maintaining the structural characteristics observed in artist-created meshes. These predicted positions are projected to their nearest surface triangle vertices and used as positional constraints in a modified Quadric Error Metrics (QEM) simplification process [Garland and Heckbert 1997].

#### 4.2 Inner skeletal joints

Character animation in modern digital content creation relies heavily on skeletal rigs, which provide intuitive control mechanisms for artists to create natural movements and poses. While manual rigging remains common practice, the increasing demand for 3D character content necessitates automated solutions for skeleton generation. Our second application addresses this need by transforming surface geometry into meaningful skeletal joint positions.

Given an input character mesh  $\mathcal{M}$ , we employ our PDT framework to predict joint positions that reside within the shape volume. The framework processes surface samples  $\mathbf{P}_{\text{ref}}$  from the input mesh, learning to transform these external points into internal skeletal joints that capture the character’s anatomical structure. Our method learns to position joints at semantically meaningful locations, such as articulation points and medial regions.

#### 4.3 Continuous feature lines

Feature line extraction from garment point clouds enables designers to understand garment construction, identify style elements, and analyze pattern layouts.

Given a dense point cloud sampling of a garment surface  $\mathbf{P}_{\text{ref}}$ , our framework transforms these input points into points on the continuous feature lines that delineate important structural elements such as stitches between patterns and boundaries. The PDT framework learns to identify and connect points that lie along meaningful feature paths, producing dense line approximations that capture both local details and global garment structure.

### 5 Experiments

#### 5.1 Experimental setups

We evaluate our PDT framework across three distinct tasks mentioned above: surface remeshing, skeletal joint prediction, and garment feature line extraction. We use standard DDPM with 1000 denoising steps. All generated keypoints are clustered with a simple thresholding.

**5.1.1 Remeshing.** For the remeshing task, we train our diffusion model on the Objaverse dataset [Deitke et al. 2023], preserving original mesh structures to maintain artist-designed priors. We curate the dataset by filtering out meshes with more than 8,192 vertices or poor mesh quality, resulting in approximately  $\sim 80k$  training meshes and  $\sim 500$  test meshes. During training, we uniformly sample 8,192 points from each input mesh surface. Our architecture employs a DiT model with 24 layers, 12 attention heads, and a hidden dimension of 768. The predicted keypoints serve as inputs to a constrained QEM algorithm [Garland and Heckbert 1997] for final

mesh generation. The model is trained on 8 NVIDIA A6000 GPUs for  $\sim 7$  days.

**5.1.2 Skeletal Joints.** For skeletal joint prediction, we utilize the ModelsResource RigNetv1 dataset [Xu et al. 2020, 2019], which comprises diverse articulated 3D characters including humanoids and animals. The dataset contains 2,163 training samples and 270 test samples. We sample 2,048 points uniformly from each input character mesh. Our implementation uses a DiT model configured with 8 layers, 8 attention heads, and a hidden dimension of 512. The model is trained on 2 NVIDIA 3090 GPUs for  $\sim 2$  days.

**5.1.3 Garment feature lines.** For garment feature line extraction, we leverage the GarmentCode dataset [Korosteleva et al. 2024; Korosteleva and Sorkine-Hornung 2023], which provides synthetic 3D made-to-measure garments with corresponding sewing patterns. The dataset features diverse garment categories fitted to various body shapes with different textile materials. We randomly sample a subset comprising 9,000 training samples and 1,000 test samples. Each garment is represented by 2,048 uniformly sampled surface points. The DiT model architecture consists of 8 layers, 8 attention heads, and a hidden dimension of 512. The model is trained on 2 NVIDIA 3090 GPUs for  $\sim 2$  days.

#### 5.2 Comparisons: remeshing

We evaluate our model’s effectiveness in mesh generation through comprehensive comparisons with state-of-the-art remeshing algorithms, including the Blender remeshing tool [Community 2018], Quadric Error Metrics (QEM) [Garland and Heckbert 1997], CWF [Xu et al. 2024], and Spectral remeshing [Lescoat et al. 2020]. All quantitative metrics are computed by uniformly sampling 8,192 points from both the input mesh and simplified mesh surfaces, and averaged over the test dataset.

**5.2.1 Qualitative analysis.** Fig. 4 presents a visual comparison of remeshing results across different methods. The leftmost column shows the vertex positions predicted by our diffusion model, demonstrating how our approach strategically places vertices to capture key structural features. In contrast to baseline methods that often produce irregular mesh structures, our method generates more coherent and structurally-aligned meshes.

**5.2.2 Quantitative evaluation.** Table 1 presents a comprehensive quantitative comparison using standard geometric fidelity metrics: Chamfer Distance (CD), Maximum Mean Discrepancy (MMD) and Coverage (COV) [Achlioptas et al. 2018], and 1-Nearest Neighbor Accuracy (1-NNA) [Lopez-Paz and Oquab 2016]. Additionally, we compare the mesh complexity in terms of vertex count (#V) and face count (#F). Our method achieves competitive metrics in all categories.

We also conducted a user study with 24 participants comparing results from QEM, CWF, Spectral, and our method across 8 representative meshes. Participants rated each result based on sharp-feature preservation, artist-like mesh quality, and overall visual appeal. Our method was preferred in all aspects against existing methods.

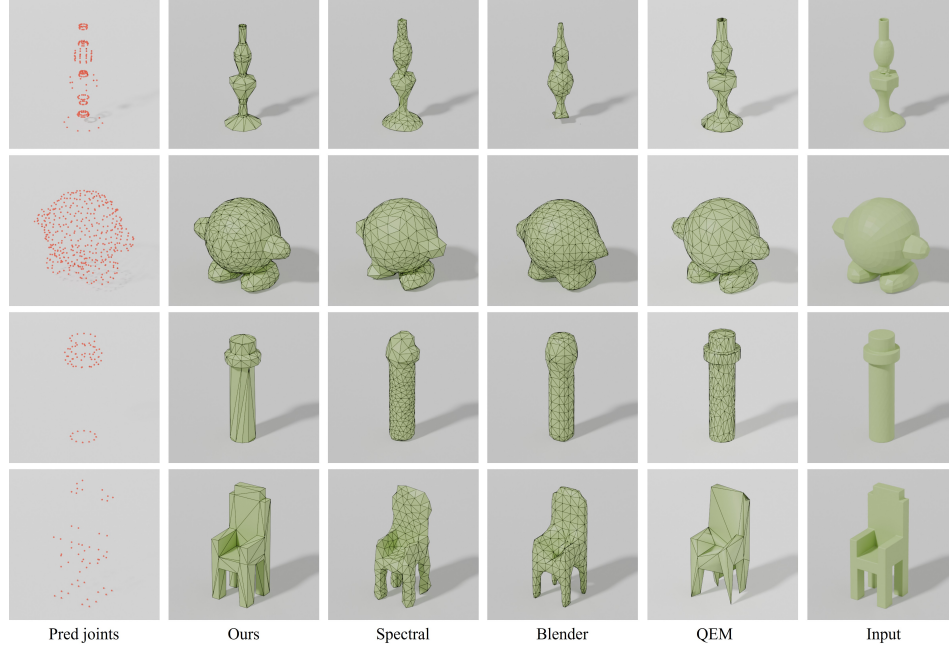


Fig. 4. Visual comparison of remeshing results across different methods. The left-most column demonstrates our method’s predicted vertex positions, which guide the subsequent mesh generation process. Note how our method preserves key structural features while maintaining regular mesh patterns.

Table 1. Quantitative comparison with existing remeshing methods.

Method	CD( $\times 10^{-2}$ ) ↓	MMD( $\times 10^{-2}$ ) ↓	COV ↑	1-NNA ↓	#V	#F
QEM	3.11	1.22	<b>0.56</b>	<b>0.56</b>	103	203
Blender	5.62	1.39	0.47	0.83	275	543
Spectral	4.50	1.20	0.51	0.74	269	546
CWF	5.52	2.12	0.52	0.69	124	250
Ours	<b>2.82</b>	<b>1.10</b>	0.53	0.72	106	201

Table 2. User study from 24 users in terms of sharp-feature preservation, artist-like mesh quality, and overall visual appeal. The number means the percentage of users favoring a specific method.

Favourite (% , ↑)	CWF	QEM	Spectral	Ours
Sharp Feature	14.1	15.1	1.0	<b>69.8</b>
Artist-like	12.0	9.4	6.8	<b>77.1</b>
Overall Visual	13.1	12.0	2.0	<b>74.3</b>

### 5.3 Comparisons: skeletal joints

We evaluate our method’s performance in skeletal joints prediction against two state-of-the-art rigging methods: Pinocchio [Baran and Popović 2007] and RigNet [Xu et al. 2020].

We employ four complementary metrics to comprehensively assess joint prediction accuracy: CD-J2J measures the average bi-directional distance between each predicted joint and its nearest reference joint (and vice versa); Intersection over Union (IoU) quantifies skeleton similarity by computing the ratio of matched joints (using Hungarian matching) within a distance tolerance (in our case, 0.1) to the total number of joints; Precision (Prec) represents the

Table 3. Comparison of joint prediction accuracy across different methods. Our method achieves better performance in all categories.

Method	CD-J2J( $\times 10^{-3}$ ) ↓	IoU ↑	Prec ↑	Rec ↑
Pinocchio	9.01	53.0%	72.1%	64.6%
Rignet	7.62	47.0%	70.4%	60.7%
Ours	<b>6.24</b>	<b>57.5%</b>	<b>84.8%</b>	<b>65.2%</b>

fraction of predicted joints that match to reference joints within the tolerance, while Recall (Rec) indicates the fraction of reference joints that match to predicted joints within the same tolerance. As shown in Table 3, our method demonstrates superior performance across all evaluation criteria.

Fig. 5 provides visual comparisons of joint prediction results across different methods. While Pinocchio [Baran and Popović 2007] and RigNet [Xu et al. 2020] sometimes misses joint positions at critical positions such as ankles and knees, our method produces more complete skeleton structures with higher accuracy.

### 5.4 Discussions

**5.4.1 Noise schedule.** We conduct a comparative analysis of three distinct noise schedules: the linear schedule proposed in the original DDPM [Ho et al. 2020], a warmup schedule where it starts slowly and then grows faster linearly, and our proposed exponential schedule. To evaluate their effectiveness for surface mesh keypoint generation, we train identical models under each schedule while maintaining all other setups constant.

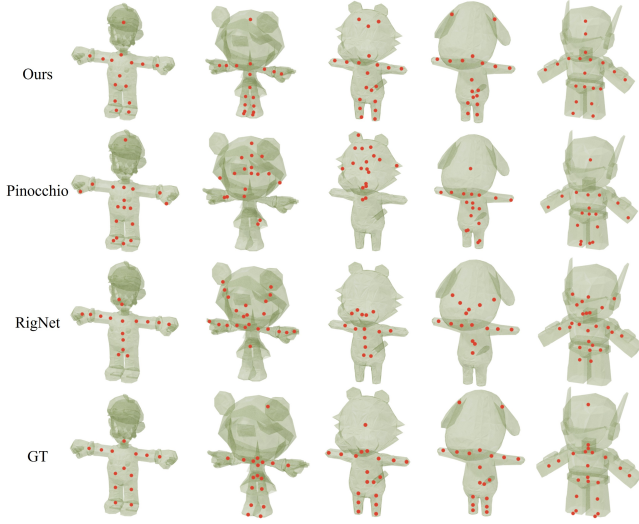


Fig. 5. Visual comparisons between joint prediction results. Our method demonstrates better alignment with the underlying geometry and more anatomically plausible skeletal structures compared to baseline methods.

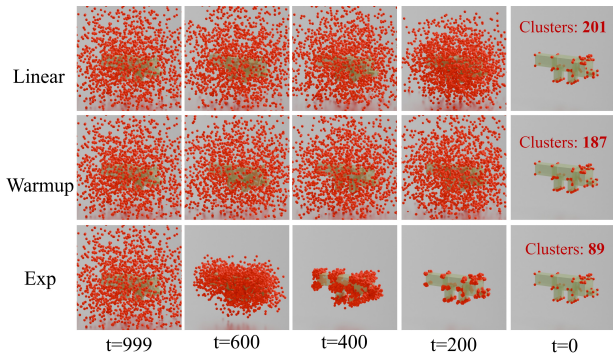


Fig. 6. Visualization of the denoising progressions. The linear and warmup schedules exhibit abrupt transitions from noise to final output, while our exponential schedule demonstrates a gradual denoising process that yields tightly consolidated points with less clusters after thresholding.

Fig. 6 illustrates the progression of the denoising process under each schedule. The visualization reveals that both linear and warmup schedules produce “fuzzy” regions where points fail to form distinct, well-separated clusters at target locations. In contrast, our exponential schedule generates tightly clustered point distributions that precisely converge to target positions, achieving less number of clusters after thresholding.

**5.4.2 Sampling gradient adjustment.** We analyze the effectiveness of our sampling gradient adjustment (SGA) mechanism in improving the geometric accuracy of predicted points. Without SGA, predicted keypoints exhibit noticeable deviation from the mesh surface. With SGA enabled, we observe consistently tighter surface adherence, with lower distance to surface as shown in Fig. 7 (left). skeletal joints predicted with SGA are also more accurately positioned at

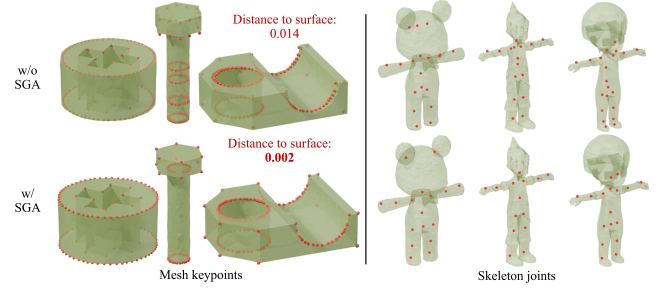


Fig. 7. Impact of sampling gradient adjustment (SGA) on point placement accuracy. Left: Surface keypoint predictions with and without SGA, showing improved surface alignment. Right: Skeletal joint predictions, demonstrating enhanced medial positioning within the shape volume.

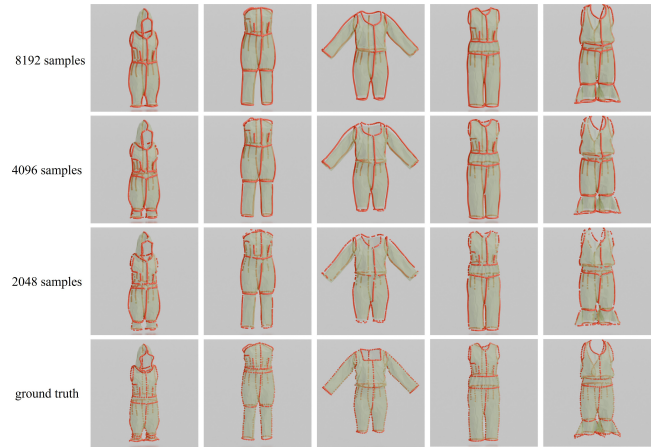


Fig. 8. Feature line extraction results with varying input sample densities. From left to right: results using  $N=2048$ , 4096, and 8192 surface points.

the medial axes of the shape, better reflecting the natural skeletal structure of the input shapes, as showcased in Fig. 7 (right).

**5.4.3 Feedforward method.** We compare our method against a PVCNN-based feedforward model [Liu et al. 2019] with more number of parameters. For skeletal joints prediction, the feedforward baseline produces an average of 56.9 joints, compared to the ground-truth average of 20.8. Their mean IoU and precision scores dropped significantly (20.0 % / 45.8% respectively). In the remeshing task, PVCNN overpredict keypoints by 700 points on average, making the outputs unsuitable for constraint-based simplification. These results underscore the importance of our point-wise guided diffusion process and exponential noise schedule for generating sparse, semantically aligned structures.

**5.4.4 Sampling points number.** While our model is trained on ground truth data containing 2048 sparse feature line points, it demonstrates effective generalization to higher sampling points. As shown in Fig. 8, PDT successfully learns to map surface points to their nearest target feature line positions, maintaining consistent quality even with significantly denser inputs than seen during training.



## 6 Conclusions

We propose PDT, a novel framework that employs diffusion models for point distribution transformation. Given an input set of points, PDT learns to transform from the original geometric distribution to a semantically meaningful target distribution. The framework's unique architecture and a set of novel designs enable diffusion models to effectively link the source and target point distributions through a denoising process. Our method is validated through three tasks, each involving the transformation of input points into distinct semantically meaningful geometric distributions: 1) surface-aligned mesh keypoints, 2) inner skeletal joints, and 3) continuous feature lines. Extensive experiments demonstrate that our method excels at generating diverse structurally meaningful point distributions through learned transformations. The proposed framework serves as a versatile solution, capable of being applied to a wide range of point cloud distribution learning and transformation tasks.

## Acknowledgments

We would like to thank the anonymous reviewers, committee members for their insightful comments and suggestions. Jionghao Wang, Wenping Wang and Xin Li are partially supported by National Science Foundation (CBET-2115405). Rui Xu, Zhiyang Dou and Taku Komura are partially supported by the Research Grants Council of Hong Kong (Ref: 17210222), the Innovation and Technology Commission of the HKSAR Government under the ITSP-Platform grants (Ref: ITS/319/21FP, ITS/335/23FP), and the InnoHK initiative (TransGP project). Rui Xu, Zhiyang Dou and Taku Komura conduct part of the research in the JC STEM Lab of Robotics for Soft Materials, funded by The Hong Kong Jockey Club Charities Trust.

## References

- Josh Achiam, Steven Adler, Sandhini Agarwal, Lama Ahmad, Ilge Akkaya, Florencia Leoni Aleman, Diogo Almeida, Janko Altmenschmidt, Sam Altman, Shyamal Anadkat, et al. 2023. Gpt-4 technical report. *arXiv preprint arXiv:2303.08774* (2023).
- Panos Achlioptas, Olga Diamanti, Ioannis Mitliagkas, and Leonidas Guibas. 2018. Learning representations and generative models for 3d point clouds. In *International conference on machine learning*. PMLR, 40–49.
- Ilya Baran and Jovan Popović. 2007. Automatic rigging and animation of 3d characters. *ACM Transactions on graphics (TOG)* 26, 3 (2007), 72–es.
- Zhang Biao, Jing Ren, and Peter Wonka. 2024. Geometry Distributions. (2024).
- Sijin Chen, Xin Chen, Anqi Pang, Xianfang Zeng, Wei Cheng, Yijun Fu, Fukun Yin, Yanru Wang, Zhibin Wang, Chi Zhang, et al. 2024a. MeshXL: Neural Coordinate Field for Generative 3D Foundation Models. *arXiv preprint arXiv:2405.20853* (2024).
- Yiwen Chen, Tong He, Di Huang, Weicai Ye, Sijin Chen, Jiaxiang Tang, Xin Chen, Zhongang Cai, Lei Yang, Gang Yu, et al. 2024b. MeshAnything: Artist-Created Mesh Generation with Autoregressive Transformers. *arXiv preprint arXiv:2406.10163* (2024).
- Zhen Chen, Zherong Pan, Kui Wu, Etienne Vouga, and Xifeng Gao. 2023. Robust low-poly meshing for general 3d models. *ACM Transactions on Graphics (TOG)* 42, 4 (2023), 1–20.
- Hyungjin Chung, Jeongsol Kim, Michael T Mccann, Marc L Klasky, and Jong Chul Ye. 2022. Diffusion posterior sampling for general noisy inverse problems. *arXiv preprint arXiv:2209.14687* (2022).
- Blender Online Community. 2018. *Blender - a 3D modelling and rendering package*. Blender Foundation, Stichting Blender Foundation, Amsterdam. <http://www.blender.org>
- Matt Deitke, Dustin Schwenk, Jordi Salvador, Luca Weihs, Oscar Michel, Eli VanderBilt, Ludwig Schmidt, Kiana Ehsani, Aniruddha Kembhavi, and Ali Farhadi. 2023. Objaverse: A universe of annotated 3d objects. In *Proceedings of the IEEE/CVF Conference on Computer Vision and Pattern Recognition*. 13142–13153.
- Qiang Du, Vance Faber, and Max Gunzburger. 1999. Centroidal Voronoi tessellations: Applications and algorithms. *SIAM review* 41, 4 (1999), 637–676.
- Xingyi Du, Xiaohan Liu, Dong-Ming Yan, Caigui Jiang, Juntao Ye, and Hui Zhang. 2018. Field-Aligned Isotropic Surface Remeshing. In *Computer Graphics Forum*, Vol. 37, 343–357.
- John Edwards, Wenping Wang, and Chandrajit Bajaj. 2013. Surface segmentation for improved remeshing. In *Proceedings of the 21st International Meshing Roundtable*. 403–418.
- Xiao Fu, Wei Yin, Mu Hu, Kaixuan Wang, Yuexin Ma, Ping Tan, Shaojie Shen, Dahua Lin, and Xiaoxiao Long. 2024. Geowizard: Unleashing the diffusion priors for 3d geometry estimation from a single image. In *European Conference on Computer Vision*. Springer, 241–258.
- Michael Garland and Paul S Heckbert. 1997. Surface simplification using quadric error metrics. In *Proceedings of the 24th annual conference on Computer graphics and interactive techniques*. 209–216.
- Jing He, Haodong Li, Wei Yin, Yixun Liang, Leheng Li, Kaiqiang Zhou, Hongbo Zhang, Bingbing Liu, and Ying-Cong Chen. 2024a. Lotus: Diffusion-based visual foundation model for high-quality dense prediction. *arXiv preprint arXiv:2409.18124* (2024).
- Kai He, Kaixin Yao, Qixuan Zhang, Jingyi Yu, Lingjie Liu, and Lan Xu. 2024b. Dress-code: Autoregressively sewing and generating garments from text guidance. *ACM Transactions on Graphics (TOG)* 43, 4 (2024), 1–13.
- Jonathan Ho, Ajay Jain, and Pieter Abbeel. 2020. Denoising diffusion probabilistic models. *Advances in neural information processing systems* 33 (2020), 6840–6851.
- Jihyeon Je, Jiayi Liu, Guandao Yang, Boyang Deng, Shengqu Cai, Gordon Wetzstein, Or Litany, and Leonidas Guibas. 2024. Robust Symmetry Detection via Riemannian Langevin Dynamics. In *SIGGRAPH Asia 2024 Conference Papers*. 1–11.
- Maria Korosteleva, Timur Levent Kesdogan, Fabian Kemper, Stephan Wenninger, Jasmin Koller, Yuhang Zhang, Mario Botsch, and Olga Sorkine-Hornung. 2024. Garment-CodeData: A Dataset of 3D Made-to-Measure Garments With Sewing Patterns. In *Computer Vision – ECCV 2024*.
- Maria Korosteleva and Olga Sorkine-Hornung. 2023. GarmentCode: Programming Parametric Sewing Patterns. *ACM Transaction on Graphics* 42, 6 (2023), 16 pages. doi:10.1145/3618351 SIGGRAPH ASIA 2023 issue.
- Thibault Lescoat, Hsueh-Ti Derek Liu, Jean-Marc Thiery, Alec Jacobson, Tamy Boubekeur, and Maks Ovsjanikov. 2020. Spectral mesh simplification. In *Computer Graphics Forum*, Vol. 39. Wiley Online Library, 315–324.
- Bruno Lévy and Yang Liu. 2010. Lp centroidal voronoi tessellation and its applications. *ACM Transactions on Graphics (TOG)* 29, 4 (2010), 1–11.
- Peng Li, Yuan Liu, Xiaoxiao Long, Feihu Zhang, Cheng Lin, Mengfei Li, Xingqun Qi, Shanghang Zhang, Wenhan Luo, Ping Tan, et al. 2024. Era3D: High-Resolution Multiview Diffusion using Efficient Row-wise Attention. *arXiv preprint arXiv:2405.11616* (2024).
- Zhouyingcheng Liao, Jimei Yang, Jun Saito, Gerard Pons-Moll, and Yang Zhou. 2022. Skeleton-free pose transfer for stylized 3d characters. In *European Conference on Computer Vision*. Springer, 640–656.
- Cheng Lin, Changjian Li, Yuan Liu, Nenglu Chen, Yi-King Choi, and Wenping Wang. 2021. Point2skeleton: Learning skeletal representations from point clouds. In *Proceedings of the IEEE/CVF conference on computer vision and pattern recognition*. 4277–4286.
- Chen Liu, Weiwei Xu, Yin Yang, and Huamin Wang. 2024. Automatic Digital Garment Initialization from Sewing Patterns. *ACM Transactions on Graphics (TOG)* 43, 4 (2024), 1–12.
- Hsueh-Ti Derek Liu, Mark Gillespie, Benjamin Chislett, Nicholas Sharp, Alec Jacobson, and Keenan Crane. 2023. Surface simplification using intrinsic error metrics. *ACM Transactions on Graphics (TOG)* 42, 4 (2023), 1–17.
- Zhijian Liu, Haotian Tang, Yujun Lin, and Song Han. 2019. Point-voxel cnn for efficient 3d deep learning. *Advances in neural information processing systems* 32 (2019).
- Xiaoxiao Long, Yuan-Chen Guo, Cheng Lin, Yuan Liu, Zhiyang Dou, Lingjie Liu, Yuexin Ma, Song-Hai Zhang, Marc Habermann, Christian Theobalt, et al. 2024. Wonder3D: Single image to 3d using cross-domain diffusion. In *Proceedings of the IEEE/CVF Conference on Computer Vision and Pattern Recognition*. 9970–9980.
- Xiaoxiao Long, Cheng Lin, Lingjie Liu, Yuan Liu, Peng Wang, Christian Theobalt, Taku Komura, and Wenping Wang. 2023. Neuraludf: Learning unsigned distance fields for multi-view reconstruction of surfaces with arbitrary topologies. In *Proceedings of the IEEE/CVF Conference on Computer Vision and Pattern Recognition*. 20834–20843.
- David Lopez-Paz and Maxime Oquab. 2016. Revisiting classifier two-sample tests. *arXiv preprint arXiv:1610.06545* (2016).
- Shentong Mo, Enze Xie, Ruihang Chu, Lanqing Hong, Matthias Niessner, and Zhenguo Li. 2023. Dit-3d: Exploring plain diffusion transformers for 3d shape generation. *Advances in neural information processing systems* 36 (2023), 67960–67971.
- Alex Nichol, Heewoo Jun, Pratul Dharwal, Pamela Mishkin, and Mark Chen. 2022. Point-e: A system for generating 3d point clouds from complex prompts. *arXiv preprint arXiv:2212.08751* (2022).
- Alexander Quinn Nichol and Pratul Dharwal. 2021. Improved denoising diffusion probabilistic models. In *International conference on machine learning*. PMLR, 8162–8171.
- Hiroemu Ozaki, Fumihito Kyota, and Takashi Kanai. 2015. Out-of-Core Framework for QEM-based Mesh Simplification. In *EuroVis*. 87–96.
- Dakshata Panchal and Deepak Jayaswal. 2022. Feature sensitive geometrically faithful highly regular direct triangular isotropic surface remeshing. *Sādhanā* 47, 2 (2022),



- 94.
- William Peebles and Saining Xie. 2023. Scalable diffusion models with transformers. In *Proceedings of the IEEE/CVF International Conference on Computer Vision*. 4195–4205.
- Charles R Qi, Or Litany, Kaiming He, and Leonidas J Guibas. 2019. Deep hough voting for 3d object detection in point clouds. In *proceedings of the IEEE/CVF International Conference on Computer Vision*. 9277–9286.
- Feng Sun, Yi-King Choi, Wenping Wang, Dong-Ming Yan, Yang Liu, and Bruno Lévy. 2011. Obtuse triangle suppression in anisotropic meshes. *Computer Aided Geometric Design* 28, 9 (2011), 537–548.
- Jiaxiang Tang, Zhaoxi Chen, Xiaokang Chen, Tengfei Wang, Gang Zeng, and Ziwei Liu. 2025. Lgm: Large multi-view gaussian model for high-resolution 3d content creation. In *European Conference on Computer Vision*. Springer, 1–18.
- Arash Vahdat, Francis Williams, Zan Gojcic, Or Litany, Sanja Fidler, Karsten Kreis, et al. 2022. Lion: Latent point diffusion models for 3d shape generation. *Advances in Neural Information Processing Systems* 35 (2022), 10021–10039.
- Yiqun Wang, Dong-Ming Yan, Xiaohan Liu, Chengcheng Tang, Jianwei Guo, Xiaopeng Zhang, and Peter Wonka. 2018. Isotropic surface remeshing without large and small angles. *IEEE Transactions on Visualization and Computer Graphics* 25, 7 (2018), 2430–2442.
- Zhengyi Wang, Jonathan Lorraine, Yikai Wang, Hang Su, Jun Zhu, Sanja Fidler, and Xiaohui Zeng. 2024. LLaMA-Mesh: Unifying 3D Mesh Generation with Language Models. *arXiv preprint arXiv:2411.09595* (2024).
- Jin Wei and Yu Lou. 2010. Feature preserving mesh simplification using feature sensitive metric. *Journal of Computer Science and Technology* 25, 3 (2010), 595–605.
- Xin Wen, Peng Xiang, Zhizhong Han, Yan-Pei Cao, Pengfei Wan, Wen Zheng, and Yu-Shen Liu. 2021. Pmp-net: Point cloud completion by learning multi-step point moving paths. In *Proceedings of the IEEE/CVF conference on computer vision and pattern recognition*. 7443–7452.
- Haohan Weng, Yikai Wang, Tong Zhang, CL Chen, and Jun Zhu. 2024. PivotMesh: Generic 3D Mesh Generation via Pivot Vertices Guidance. *arXiv preprint arXiv:2405.16890* (2024).
- Rui Xu, Longdu Liu, Ningna Wang, Shuangmin Chen, Shiqing Xin, Xiaohu Guo, Zichun Zhong, Taku Komura, Wenping Wang, and Changhe Tu. 2024. CWF: Consolidating Weak Features in High-quality Mesh Simplification. *ACM Transactions on Graphics (TOG)* 43, 4 (2024), 1–14.
- Zhan Xu, Yang Zhou, Evangelos Kalogerakis, Chris Landreth, and Karan Singh. 2020. Rignet: Neural rigging for articulated characters. *arXiv preprint arXiv:2005.00559* (2020).
- Zhan Xu, Yang Zhou, Evangelos Kalogerakis, and Karan Singh. 2019. Predicting animation skeletons for 3d articulated models via volumetric nets. In *2019 international conference on 3D vision (3DV)*. IEEE, 298–307.
- Dong-Ming Yan and Peter Wonka. 2015. Non-obtuse remeshing with centroidal Voronoi tessellation. *IEEE Transactions on Visualization and Computer Graphics* 22, 9 (2015), 2136–2144.
- Kangxue Yin, Hui Huang, Daniel Cohen-Or, and Hao Zhang. 2018. P2p-net: Bidirectional point displacement net for shape transform. *ACM Transactions on Graphics (TOG)* 37, 4 (2018), 1–13.
- Zhengming Yu, Zhiyang Dou, Xiaoxiao Long, Cheng Lin, Zekun Li, Yuan Liu, Norman Müller, Taku Komura, Marc Habermann, Christian Theobalt, et al. 2023. Surf-D: High-Quality Surface Generation for Arbitrary Topologies using Diffusion Models. *arXiv preprint arXiv:2311.17050* (2023).
- Biao Zhang, Jiapeng Tang, Matthias Niessner, and Peter Wonka. 2023. 3dshape2vecset: A 3d shape representation for neural fields and generative diffusion models. *ACM Transactions on Graphics (TOG)* 42, 4 (2023), 1–16.
- Longwen Zhang, Ziyu Wang, Qixuan Zhang, Qiwei Qiu, Anqi Pang, Haoran Jiang, Wei Yang, Lan Xu, and Jingyi Yu. 2024. CLAY: A Controllable Large-scale Generative Model for Creating High-quality 3D Assets. *ACM Transactions on Graphics (TOG)* 43, 4 (2024), 1–20.
- Linqi Zhou, Yilun Du, and Jiajun Wu. 2021. 3d shape generation and completion through point-voxel diffusion. In *Proceedings of the IEEE/CVF international conference on computer vision*. 5826–5835.

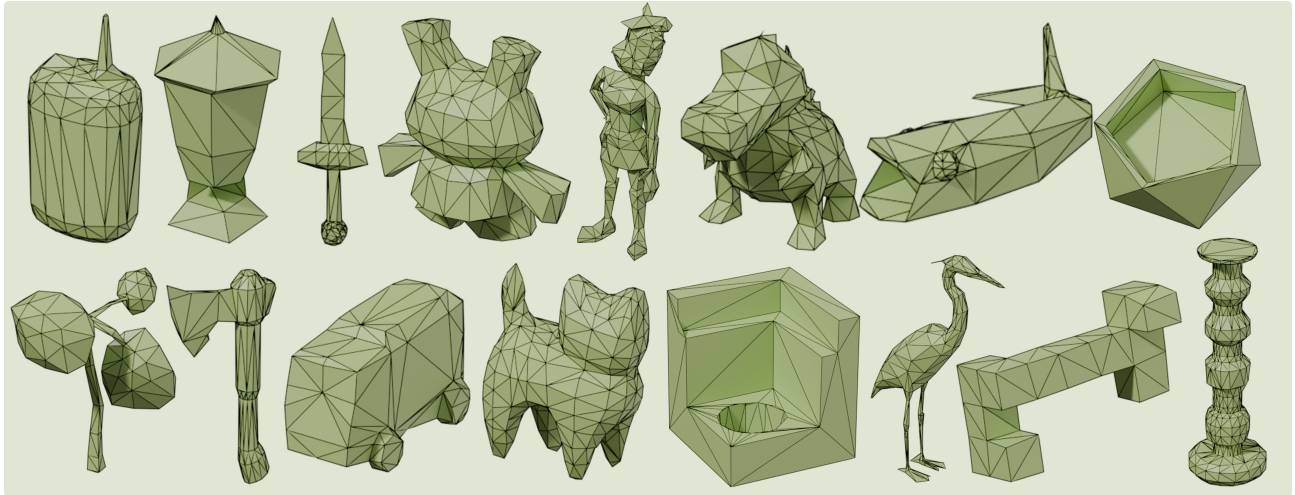


Fig. 9. Gallery of our remeshing results.

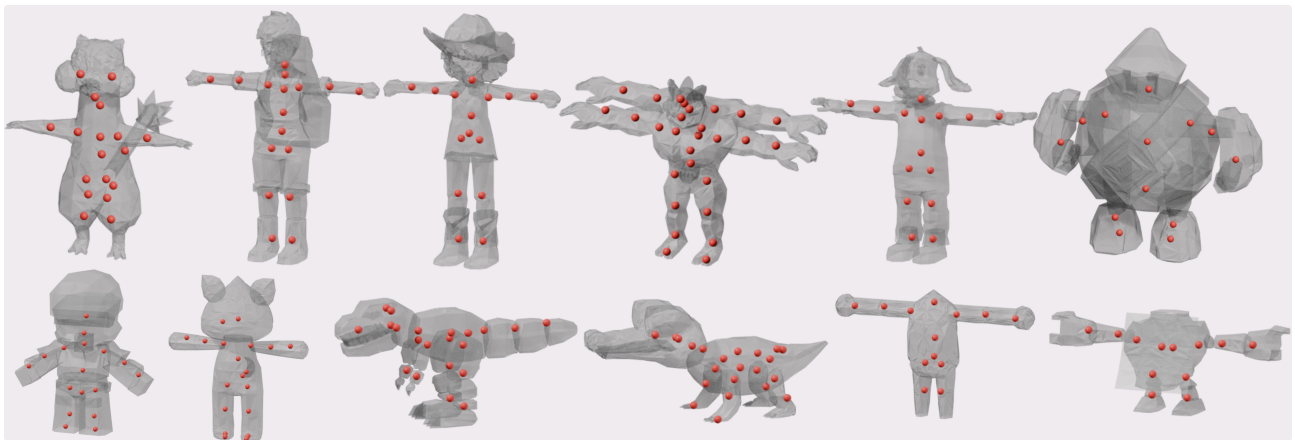


Fig. 10. Gallery of our skeletal joints results.



Fig. 11. Gallery of our garment feature line extraction results.